International Journal of Nanomedicine

Dovepress
open access to scientific and medical research

Open Access Full Text Article

ORIGINAL RESEARCH

Self-Assembled Nano-Peptide Hydrogels with Human Umbilical Cord Mesenchymal Stem Cell Spheroids Accelerate Diabetic Skin Wound Healing by Inhibiting Inflammation and Promoting Angiogenesis

Junshuai Xue[1], Nianfeng Sun[2], Yang Liu[3]

[1]Department of General Surgery, Qilu Hospital of Shandong University, Jinan City, Shandong Province, People's Republic of China; [2]Women's and Children's Hospital Affiliated to Qingdao University, Qingdao, 266001, People's Republic of China; [3]Department of General Surgery, Vascular Surgery, Qilu Hospital of Shandong University, Jinan City, Shandong Province, People's Republic of China

Correspondence: Nianfeng Sun; Yang Liu, Tel +86 18561810688; +86 18560088317, Email sunnianfeng@126.com; liuyang_sdu@126.com

Background: Non-healing skin wounds are a common complication in diabetic patients. Vector biomaterials embedded with mesenchymal stem cells (MSCs) are considered a promising treatment approach. In this study, we presented a novel and effective approach to accelerate diabetic skin wound healing.

Methods and Materials: Human umbilical cord mesenchymal stem cells (hUC-MSCs) were shaped into spheres. RADA16-I, KLT, and RGD nanopeptides were selected for self-assembly into hydrogels. hUC-MSCs spheroids (hUC-MSCsp) were combined in vitro with self-assembled nanopeptide hydrogels and subsequently transplanted into a mouse model of diabetic skin trauma.

Results: Compared with the PBS, hUC-MSCs, hUC-MSCsp, and hUC-MSCs with hydrogel groups, hUC-MSCsp with hydrogel significantly accelerated wound healing ($p<0.01$) and shortened the healing time (10 vs 14 vs 21 days). The expressions of IL-6, IL-10, IL-1β, and TNF-α were significantly decreased ($p<0.001$). The expression of VEGF was significantly higher in the hUC-MSCsp with hydrogel group ($p<0.05$), and the density of neovascularization in the fresh skin tissue at the wound was also remarkably increased ($p<0.01$).

Conclusion: Nanopeptide hydrogels loaded with hUC-MSCsp accelerated diabetic skin wound healing by inhibiting inflammation and promoting angiogenesis compared with conventional stem cell transplantation, which deserves further investigation.

Keywords: diabetic wound, human umbilical cord mesenchymal stem cell, spheroid, nanopeptide hydrogels, treatment

Introduction

Diabetes mellitus (DM) is a disorder of carbohydrate, protein and fat metabolism caused by the absolute or relative insufficiency of insulin secretion or impaired insulin utilization, and is characterized by hyperglycemia.[1,2] With the progression of the disorder, the diabetic will gradually exhibit multi-system damage, often resulting in such conditions as cardiovascular disease, blindness, kidney failure, and amputation. Extremity skin infection and ulcer are serious complications in the late stage, which seriously affects the quality of life of diabetic patients.[3] Diabetic skin wound healing is a complex process that involves inflammation, proliferation, and remodeling, and these three phases overlap each other closely, in which inflammation plays a key role.[4] Therefore, in addition to controlling hyperglycemia and eliminating necrotic tissue, the management of inflammation and the improvement of blood circulation are crucial for the treatment of diabetic skin wounds.[5]

Mesenchymal stem cells (MSCs) with multidirectional differentiation potential and self-renewal capability, are widely present in a variety of tissues. Currently, damaged tissues are often repaired by transplanting MSCs directly into target

Received: 23 February 2022
Accepted: 23 May 2022
Published: 30 May 2022

tissues or by stimulating MSCs into mature tissues.[6,7] However, the autocrine/paracrine capability of MSCs may provide a more effective approach. MSCs can be used as seed cells in combination with vector biomaterials to form a three-dimensional cell growth environment that promotes cell-cell interactions, cell-matrix interactions, and which can also perform certain physiological functions produced by tissue-specific cells within organ classes.[8] Biological carrier materials can promote the growth, secretion, and differentiation of stem cells, and these biofactors secreted by MSCs can in turn promote changes in the mechanical properties and environmental remodeling of the carrier material. Together, these interactions constitute a multicellular system with enhanced robustness and physiological relevance.[9]

Hydrogels are widely used in various tissue engineering research because of their low cost, simple synthesis, low immunoreactivity, relative stability, and tight conformational control.[10,11] Previous studies have shown that MSCs can promote the secretion of high amounts of multiple cytokines as well as immunomodulatory paracrine factors when self-assembled with hydrogels into spheroids.[12,13] In this study, we promoted the three-dimensional aggregation of human umbilical cord MSCs spheroids (hUC-MSCsp) in vitro, then pre-mixed them with self-assembled nanopeptide hydrogels and examined the expression of vascular endothelial growth factor (VEGF) and other inflammatory factors. hUC-MSCsp were transplanted into a mouse model of diabetic skin wound. The rate of wound healing was recorded and the expressions of relevant inflammatory factors, neovascular density, and specific markers were also examined.

Methods and Materials

Culture and Identity of hUC-MSCs

hUC-MSCs were purchased from Shanghai Yes Service Biotech, Inc. (China) and tested for mycoplasma contamination by PCR. hUC-MSCs were cultured in Dulbecco's Modified Eagle's Medium (DMEM)/F12 (Gibco, US) containing 10% fetal bovine serum (FBS) and 100 U mL^{-1} penicillin-streptomycin (Gibco, USA) in a 37°C incubator. After successive passages to the third generation, hUC-MSCs were identified by observing cell morphology, examining multidirectional differentiation capacity, and cell surface markers. Then, 80% of fused hUC-MSCs were digested down using 0.25% trypsin - ethylene diamine tetraacetic acid (EDTA) (Gibco, USA). The digested hUC-MSCs suspension was washed twice with phosphate buffer saline (PBS) and the cells were resuspended with 3 mL of PBS. This resulted in a highly concentrated cell suspension. The hUC-MSCs suspension was dispensed at 500 μL/tube into 6 flow-through tubes, one of which was used as a blank control. PE-labeled mouse anti-human flow antibodies to CD31, CD45, CD90, CD105, and isotype control IgG1 (BioLegend, USA) were added to each of the remaining tubes, blown and mixed and incubated for 20 minutes at room temperature, and protected from light. The tips used for adding antibodies and blow mixing were changed per tube to avoid contamination. Expression distribution was assessed by single-channel flow cytometry (BD Biosciences, USA). The antibodies were obtained from BioLegend, USA.

Multi-Directional Differentiation Capability of hUC-MSCs

The innate potential of hUC-MSCs to differentiate into osteoblasts, adipocytes and chondrocyte lineages was evaluated. In the 3rd generation, hUC-MSCs were inoculated in 6-well plates at 2×10^4 cells/cm^2 and cultured with 2 mL of complete medium. When fusion reached 100% or over fusion was achieved, hUC-MSCs were incubated in a solution containing 10% FBS, 1% penicillin-streptomycin, 0.1% dexamethasone, 0.1% 3-isobutyl-1-methylxanthine, 1% glutamine, 0.2% insulin, and 0.1% rosiglitazone, followed by a solution containing 10% FBS, 1% penicillin-streptomycin, 1% glutamine, and 0.2% insulin in a solution of biolipid differentiation medium for 3 days and in biolipid differentiation medium B for 1 day. This was alternated 3–5 times and then the culture continued in solution B for 4–7 days until the lipid droplets became sufficiently large and round. Lipid formation was detected using Oil Red O staining. When fusion reached 70%, hUC-MSCs were replaced with osteogenic induced differentiation medium containing 10% fetal bovine serum, 1% penicillin-streptomycin, 0.01% dexamethasone, 1% glutamine, 0.2% ascorbic acid, and 1% sodium β-glycerophosphate as described above. The medium was renewed every 3 days. Osteogenesis was examined 3 weeks after induction with an alizarin red staining kit. Briefly, 4×10^5 hUC-MSCs were suspended in 15 mL centrifuge tubes and centrifuged at 150 ×g for 5 minutes. Cells were deposited and cultured in chondroinduction medium containing 0.01% dexamethasone, 0.3% ascorbic acid, 1% ITS additive, 0.1% sodium pyruvate, 0.1% proline,

and 1% TGF-β3 for 3 weeks. Spheres were formed and then slightly shaken to prevent apposition. The cartilage induction medium was renewed every 3 days. The cell microspheres were fixed, cut into 4-μm sections, and stained with Alcian Blue for observation. The above reagents were purchased from Cyagen, product numbers: HUXUC-90031, 90021, and 900042.

Spherification and Transfection of hUC-MSCs

Lentivirus with green fluorescent protein (GFP) was purchased from (GKN, China, product No.: LVCON313). The 3rd generation hUC-MSCs were seeded at a density of 1×10^5/well and incubated in 6-well plates 18–24 hours before transfection. The next day, lentiviruses with GFP fluorescent markers were transfected. The number of cells at the time of transfection was approximately 3×10^5/well. The multiplicity of infection (MOI) was 20. The medium was changed after 24 hours of co-culture. Fluorescence was observed with an inverted fluorescence microscope. Based on the fluorescence intensity, cells that failed to stably express GFP were screened with 4 μg/mL of puromycin. After the stable expression of GFP was established, we examined whether cell proliferation and apoptosis were affected before and after transfection using a cell counting kit-8 (CCK-8) and apoptosis kits (Annexin V-APC and 7-AAD, Elabscience, China). Ultra-low adsorption round-bottom 96-well culture plates (Corning 7007, USA) were sterilized with UV light prior to the spheroidization of hUC-MSCs. Then, 100 μL of hUC-MSCs suspension at a concentration of 2.5×10^6/mL was added to each well and the cells were gently shaken to concentrate them at the bottom of the plate. After 48 hours of incubation, hUC-MSCs spheres were formed and removed from the wells with a pipette.

Peptide Solutions

The ion-complementary self-assembled peptide RADA16-I with the sequence (Ac-RADARADARADARADA-CONH2), the functional peptide KLT containing a VEGF mimetic fragment (GGGKLTWQELYQLKYKGI) with the sequence (GGGKLTWQELYQLKYKGI- RADARADARADARADA-NH2), and the peptide RGD with the sequence (RGDRADARADARADA-NH2) were selected (Supplementary Figure 1A, B and C). The above peptides were purchased from China Peptides. Co. Ltd. The purity and identity of the peptides were confirmed by analytical high-performance liquid chromatography and mass spectrometry, respectively. RADA16-I is a commonly used self-assembling peptide in tissue engineering.[14] The KLT peptide contains a VEGF mimetic fragment that mimics part of the helical region of VEGF, which activates VEGF receptors and VEGF-related cellular signaling pathways, to activate endothelial cell proliferation.[15] The RGD polypeptide family is thought to have a specific recognition site for integrin receptors. Integrin receptors are key regulators of cell-cell and cell-extracellular microenvironmental communication. Therefore, the RGD peptide family is considered a suitable candidate for the treatment of multiple diseases and organ regeneration in various tissues.[16] All peptide solutions were prepared with bio-grade sterile deionized water, filtered through 0.22 μm syringe-driven filters (Millipore, USA), and stored at −20°C. The initial concentration of the peptide solution was 10 mg/mL (1%). Peptide solutions for experiments were obtained by thoroughly mixing 50 μL of RADA16-I, 25 μL of RGD, and 25 μL of KLT peptide solution at a ratio of 2:1:1, followed by the addition of 900 μL of bio-grade sterile deionized water at a concentration of 1 mg/mL (0.1%).

Preparation of Self-Assembled Peptide Hydrogels

We assembled a block hydrogel with a regular shape to culture cells. Transwell chambers (Corning, China) were used to complete the self-assembly of the salt solution-induced peptide solutions. The required number of transwell chambers were placed in a 24-well culture plate with 400 μL PBS added to each well. The 24-well plates were placed in a cell culture incubator overnight to allow the basement membrane of the transwell chambers to permeate out. Then, the permeable PBS was aspirated from the chambers and 400 μL of PBS was re-added to flood the basement membrane of the chambers with PBS. Next, 100 μL of peptide solution (0.1%) was slowly added against the wall in each transwell to prevent air bubble generation. Then, the 24-well plates were placed in a cell incubator overnight to allow the PBS in the 24-well plates to slowly pass through the basement membrane of the chambers to induce the peptide solution to self-assemble and form a hydrogel. Finally, the 24-well plates were removed from the incubator and observed for the successful assembly of the peptide solution to form a hydrogel.

Rheometry Assay

Oscillatory rheology measurements were performed on an MARS60 rheometer (Thermo Fisher, Germany). First, 0.1% peptide solutions were prepared by mixing 1% (*w/v*) peptide reserve solution with PBS at a ratio of 1:9. After incubation for 5 minutes, 500 μL was loaded for analysis on a Peltier plate of the MARS60 rheometer, and the upper plate was lowered to a gap height of 50 μm. Dynamic frequency sweep tests were performed over a range of frequencies from 0.1 to 100 rad/s at a constant 1% oscillatory strain and temperature of 37°C.

Circular Dichroism (CD)

CD spectroscopy was performed on a Chirascan spectrometer (Applied Photophysics, UK). First, 0.1% peptide solutions were prepared by mixing a 1% (*w/v*) peptide reserve solution with sterile deionized water at a ratio of 1:9. Then, 400 μL was added into a CD cuvette with a 10 mm path length. CD data were acquired over a range of 190–260 nm at a bandwidth of 1.5 nm and scan speed of 20 nm/s.

Atomic Force Microscopy (AFM)

A 10 μL sample was dropped on the silicon wafer surface, air-dried, and analyzed in tapping mode by AFM (Bruker, Germany). Images were acquired with a silicon scanning probe with a resonant frequency of 300 kHz, a spring constant of 40 N/m, a tip radius curvature of 3.4 μm, a length of 125 μm, and a width of 40 μm. Typical scanning parameters were a tapping frequency of 300 kHz, a pre-engagement RMS amplitude of 122.38 Mv, a set point of 250 mV, and a scan rate of 0.727 Hz.

Scanning Electron Microscopy (SEM) and Mapping Analysis

A small chamber was removed from a 24-well culture plate and the basement membrane was cut off. The hydrogel was removed and its properties were observed. After fixation with 2.5% glutaraldehyde fixative for 30 minutes, the hydrogels were dehydrated in gradients of 70%, 80%, 90% and 100% ethanol for 10 minutes, respectively. SEM samples were prepared by dehydration followed by gold spraying, and the hydrogels were tested by scanning electron microscopy to observe their internal structures. In addition, the elemental composition of the hydrogel and its percentage were obtained by mapping analysis.

Co-Culture of hUC-MSCs with Hydrogel

Complete medium containing peptide was prepared with complete medium and 1% peptide solution at a ratio of 100:1, and then cells were inoculated into 6-well plates and cocultured at 3×10^5 cells/well. Cell viability was detected by AO/EB staining. After hUC-MSCs were co-cultured with hydrogels for 24, 48 and 72 hours, the cells were digested down by centrifugation with EDTA-containing trypsin and washed with PBS. Then, 5 μL AO and 5 μL EB solutions were added, and the morphology and color of the cell nuclei were observed under a fluorescence microscope (IX53, Olympus). An enzyme-linked immunosorbent assay (ELISA) (Elabscience, China) was used to detect the concentration of VEGF in the culture supernatant with total cellular protein. When cell fusion reached 80%, the culture supernatant was transferred to a 1.5 mL EP tube. The cells were washed with PBS 2–3 times. Cells were scraped off with a cell scraper and added to the 1.5 mL EP tube. Subsequently, radioimmunoprecipitation assay buffer (RIPA) with a phenylmethanesulfonyl fluoride (PMSF) (100:1) mixture was added. Cells were lysed on ice for 30 minutes, placed on a shaker, blown every 5 minutes, and centrifuged at 12,000 rpm for 5 minutes. The supernatant was placed into a new EP tube as the sample to be tested. The supernatant and total protein samples were added to the wells according to the instructions of the ELISA kit, and three replicate wells were set up. The concentration of VEGF in each well was measured according to the protein standard curve.

Animal Model of Diabetic Skin Wound

NOD/SCID mice (6–8 weeks old; 20–25 g) were purchased from Charles River Corporation (Beijing, China). The animal experiments were approved by the Ethics Committee of Shandong University Qilu Hospital and were conducted in accordance with the ethical guidelines and in compliance with the National Institutes of Health Guide for the Care and Use of Laboratory Animals. (ethics number: KYLL-KS-2021101)

Twenty-five mice were randomly assigned to five groups, including PBS, hUC-MSCs, hUC-MSCsp, hUC-MSCs +hydrogel, and hUC-MSCsp+hydrogel groups. Because hydrogels can directly induce self-assembly into gels in the ionic state, the cells were mixed with the peptide solution and dropped directly onto the trauma. Five mice were used in each group. After excision of the dorsal skin under anesthesia, a full thickness wound of 8 mm diameter was created on the dorsal midline. For the control group, 30 μL PBS was injected into the wound bed using a pipette. For the hUC-MSCs group, 30 μL PBS containing hUC-MSCs (1×10^6 cells) was injected into the wound bed. For the hUC-MSCsp group, 30 μL PBS containing hUC-MSCs spheroids (40 spheroids, 1×10^6cells) was administered. For the hUC-MSCs+hydrogel and hUC-MSCsp+hydrogel groups, the hydrogel was injected into the wound bed (30 μL, each wound containing 1×10^6cells and 40 spheroids, respectively). After injection, all wounds were covered with a transparent film dressing (Tegaderm Film, 3M, USA). Digital images were captured on days 0, 3, 7, 10, 14, and 21. The percentage of the original wound area at different time points was assessed by comparison with the initial wound area on the day of surgery. Healing rate was defined as (initial diameter - wound diameter)/initial diameter × 100%.

Histological Analysis and Immunohistochemical Staining

Mice were sacrificed on days 3, 7, 14, and 21 after treatment, and their skins were excised for further histological examinations. The wound area was excised and fixed in 10% paraformaldehyde. After tissue processing, the skin was embedded in paraffin and cut into 7-μm thick sections. After deparaffinization and rehydration, the prepared specimens were placed on slides and stained with hematoxylin and eosin (HE). Images were taken using an Olympus inverter. Angiogenesis in each group was detected by CD31 staining (Servicebio, China), and the role of cells in trauma by GFP staining (Abcam, USA). After a series of dewaxing, rehydration, and antigen reduction treatments, paraffin sections were incubated with primary antibody (rabbit anti-mouse) overnight at 4°C, followed by three shaker washes and secondary antibody (HRP-labeled goat anti-rabbit IgG) incubation. Subsequently, sections were incubated with diaminobenzidine (DAB) substrate to observe antibody binding. CD31 staining in the tissue was observed under a 400× microscope.

Measurement of Inflammatory Cytokine Concentrations in Tissue Samples

The concentrations of interleukin (IL)-6, IL-10, IL-1β, and tumor necrosis factor (TNF)-α in tissue samples were detected by ELISA. The tissues of each group were weighed accurately and added to 9 times the volume of homogenization medium (0.9% saline) at a ratio of weight (mg):volume (μL) = 1:9. Mechanical homogenization was performed under ice water bath conditions to prepare a 10% homogenate, centrifuged at 3000 rpm for 10 minutes, and the supernatant was used for the assay. The sample to be tested was added according to the procedure in the ELISA instructions. A standard curve was generated according to the concentration and integral optical density (IOD) value of the standards, and then the sample concentration was calculated according to the equation of the standard curve (Servicebio, China).

Statistical Analysis

The trabecular diameters of CD31-positive microvessels and the mean IOD of 3 random regions (400×) were calculated using Image-Pro Plus 6.0 software. Quantitative data were obtained with GraphPad Prism software (GraphPad Prism, version 7) unless otherwise stated, and data are expressed as the mean ± standard deviation (SD). Statistical analysis was performed by one-way analysis of variance (ANOVA) with Turkey post hoc test or *t*-test. Significance between different treatments and experimental results was determined by post hoc tests. The P-value for statistical significance was set at $p<0.05$.

Results

Identification, Transfection, and Spherification of hUC-MSCs

As shown in Figure 1B i, the 3rd generation hUC-MSCs had a spindle-shaped morphology in vitro. The results of a tri-lineage differentiation assay demonstrated the pluripotency of hUC-MSCs (Figure 1A i, ii and iii). Flow cytometry immunophenotyping showed that the isotype control was negative for IgG1, negative for an endothelial cell marker antibody (CD31), negative for a leukocyte marker antibody (CD45), and positive for other marker antibodies (CD90 and

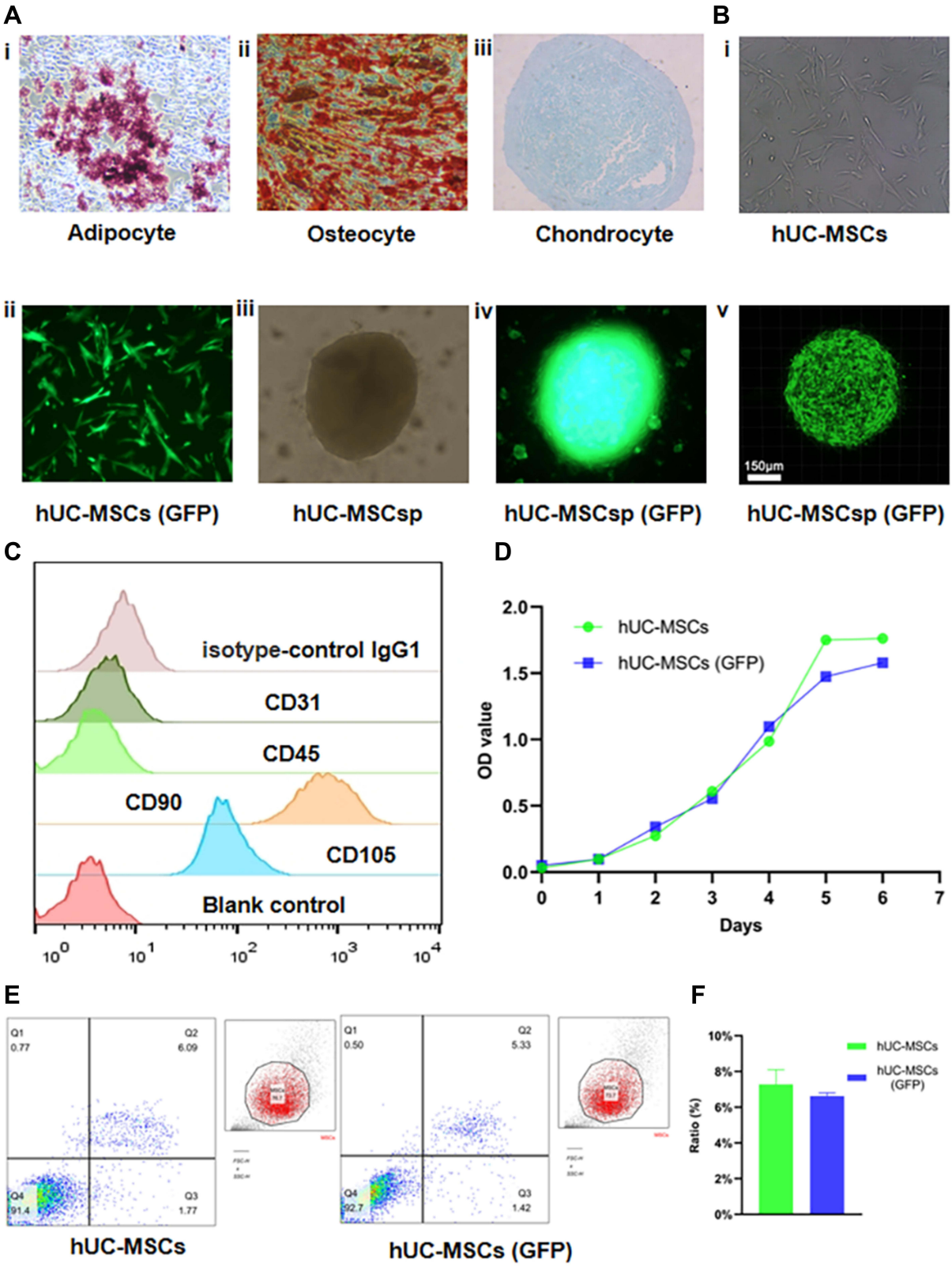

Figure 1 Identity, transfection and spherification of hUC-MSCs. (**A**) Representative images (100×) of adipogenesis (i), osteogenesis (ii), and chondrogenesis (iii) of hUC-MSCs stained with oil red O, alizarin red S, and Alcian blue, respectively. (**B**) Transfection and spherification of hUC-MSCs were performed. hUC-MSCs (GFP) (ii) were obtained by transfecting lentiviruses with GFP into hUC-MSCs (i). hUC-MSCsp (iii), and hUC-MSCsp (GFP) (iv and v) were observed by inverted fluorescent microscopy and confocal laser scanning microscopy, respectively. (**C**) Surface markers of hUC-MSCs, including isotype-control IgG negative, CD31 negative, CD45 negative, CD90 positive, and CD105 positive cells, were detected by flow analysis. (**D**) The proliferation ability of the hUC-MSCs group and hUC-MSCs (GFP) groups was detected by CCK-8 at 1 week. (**E** and **F**) Apoptosis of hUC-MSCs, hUC-MSCs, and hUC-MSCs (GFP) groups was detected by flow analysis (annexin V-APC and 7-AAD).

CD105). Therefore, the possibility of other cell types being present can be excluded.[17] Flow cytometric typing showed that the cultured cells conformed to the immunophenotypic profile of hUC-MSCs (Figure 1C). A stable expression of GFP in hUC-MSCs was obtained by transfection (Figure 1B, ii). We obtained hUC-MSCsp and hUC-MSCsp (GFP) using ultra-low adsorption round bottom 96-well culture plates (Figure 1B iii and iv). hUC-MSCsp (GFP) were observed using inverted fluorescent microscopy and confocal laser scanning microscopy (CLSM), respectively (Figure 1B iv and v). In addition, CCK-8 value-added assays were performed on transfected cells and untransfected hUC-MSCs. As shown in Figure 1D, the proliferation of hUC-MSCs transfected with GFP was unaffected at an absorbance of 460 nm, and was not statistically significant. We also tested whether transfection with GFP caused cell apoptosis or death. As shown in Figure 1E, flow cytometry data showed no difference in apoptosis between the two groups. This demonstrated that transfection with GFP was safe and feasible for hUC-MSCs (Figure 1F).

Properties of Hydrogel Scaffolds

After dissolving the peptide powder in bio-grade sterile ultra-pure water to prepare a 1% peptide solution, the peptide solution was viscous and turbid. After sufficient mixing, the peptide solution clarified, indicating it was well dissolved and mixed. After preparing AFM samples, nanofibrous structures of the peptides were detected. The morphology of the 0.1% peptide solution dissolved in deionized water was examined by AFM imaging, which showed that the three-dimensional structure had homogeneity with undulations between −10 ~ 10 nm, indicating a relatively stable hydrogel microstructure (Figure 2A). The nanofiber solutions rapidly self-assembled into hydrogel scaffolds in the presence of culture solution or ionic liquid. Macroscopic examination of the hydrogel scaffold at a concentration of 0.1% showed that the scaffold was semi-fluid and could be formed into an exact shape according to its container (Figure 2B, i). In addition, we investigated the internal structure of the peptide hydrogel scaffold using SEM, which clearly showed the three-dimensional nature and structure of the hollow cavities after hydrogel dehydration (Figure 2B ii, and iii). The hollow cavities in the hydrogel were shuttle-shaped and varied in size, providing space for the adhesion and proliferation of transplanted cells. In addition, the mapping analysis showed that the content and type of elements inside the hydrogel contained O, Na, C, P, and N in descending order of content (Figure 2C and D).

Oscillatory rheological assays were used to test the viscoelastic properties of each peptide in PBS. The energy storage modulus (G') and loss modulus (G") are related to the elasticity and viscosity of the material, respectively. The sweep results showed that the values of the storage modulus (G') were larger than the loss modulus (G") in RADA16-I (Figure 3A), KLT (Figure 3C), and RADA16-I+RGD+KLT mixtures (Figure 3D), and that G' and G" were independent of frequency. In RGD, the values of the storage modulus (G') and loss modulus (G") were similar (Figure 3B), and G' was only less than 1/10 of RADA16-I, indicating the poor ability of RGD to form gels. In contrast, the modulus of RADA16-I+RGD+KLT was significantly higher than that of RGD, indicating that the addition of RADA16-I and KLT improved the gel-forming property of RGD.

The β-sheet structure of the self-assembled peptide may be a prerequisite for the self-assembly of the peptide into nanofibers. As shown in Figure 3E, the CD spectral analysis showed a typical β-sheet structure of RADA16-I with a negative maximum at 216 nm and a positive maximum at 199 nm. In the analysis of the RADA16-I+RGD+KLT mixture, the lines had a similar trend with the change in wavelength. There was a negative maximum at 214 nm and a positive maximum at 192 nm. Therefore, despite the addition of RGD and KLT peptides, the mixed peptide solution was stable and did not change significantly compared with the single RADA16-I solution, which was consistent with the storage modulus (G') and loss modulus (G") observed in the rheological analysis.

Properties of Hydrogel Loaded with hUC-MSCs

After hUC-MSCs were co-cultured with hydrogels for 24, 48 and 72h, the cells were stained with AO/EB. As shown in Figure 2E, live cells were stained with green fluorescence and dead cells were stained with red fluorescence (magnification: 400×). Few apoptotic cells (orange fluorescence, counted after removing cell debris) were observed indicating that the cells grew and survived within the hydrogel and showed good biocompatibility. Furthermore, an intergroup analysis revealed that the concentration of total intracellular protein VEGF in the complete medium co-cultured with the hydrogels was higher than that in the complete medium supernatant only. Intra-group analysis showed that the

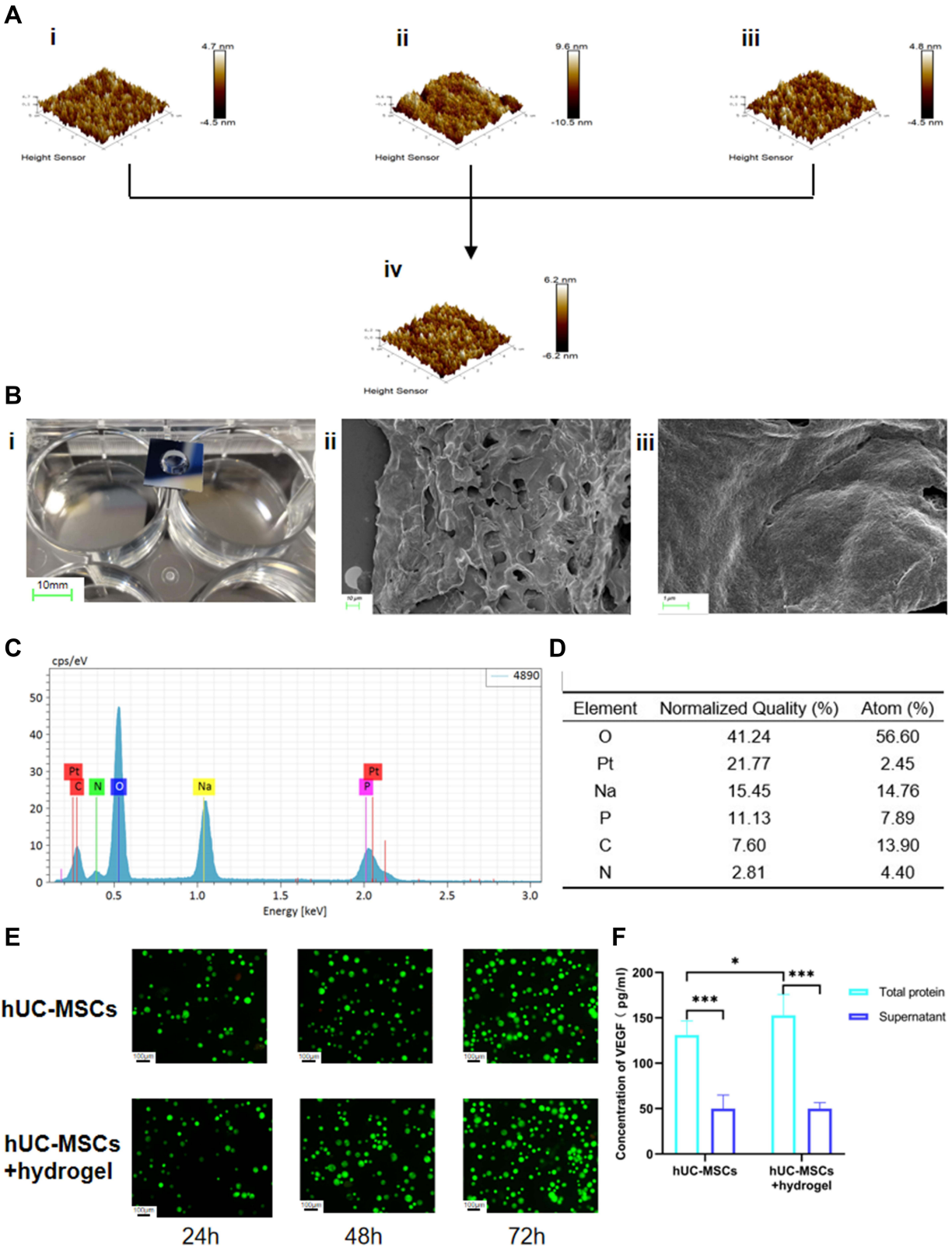

Figure 2 Characteristics of peptide hydrogel and co-culture with hUC-MSCs. (**A**) Microstructure of peptide hydrogel including RADA16-I (i), RGD (ii), KLT (iii), and mixed peptide hydrogel (iv) were observed by atomic force microscopy. (**B**) Macrostructure of a self-assembled mixed peptide hydrogel using a transwell chamber (Corning 7007). Scale bar: 10 mm (i) Microstructure of a mixed peptide hydrogel was observed using scanning electron microscopy. Scale bar: 10 μm (ii) and 1 μm (iii). (**C** and **D**) The elemental composition of the mixed peptide hydrogel and their percentages were obtained by mapping analysis. (**E**) The state of the mixed peptide hydrogel co-cultured with hUC-MSCs in hUC-MSCs and hUC-MSCs+hydrogel groups was examined by AO/EB staining after 24, 48, and 72h. (**F**) The concentration of VEGF in the total protein and supernatant after co-culture of hUC-MSCs with or without mixed peptide hydrogels was measured with a VEGF kit. Scale bar: 100 μm. *p<0.05, ***p<0.001.

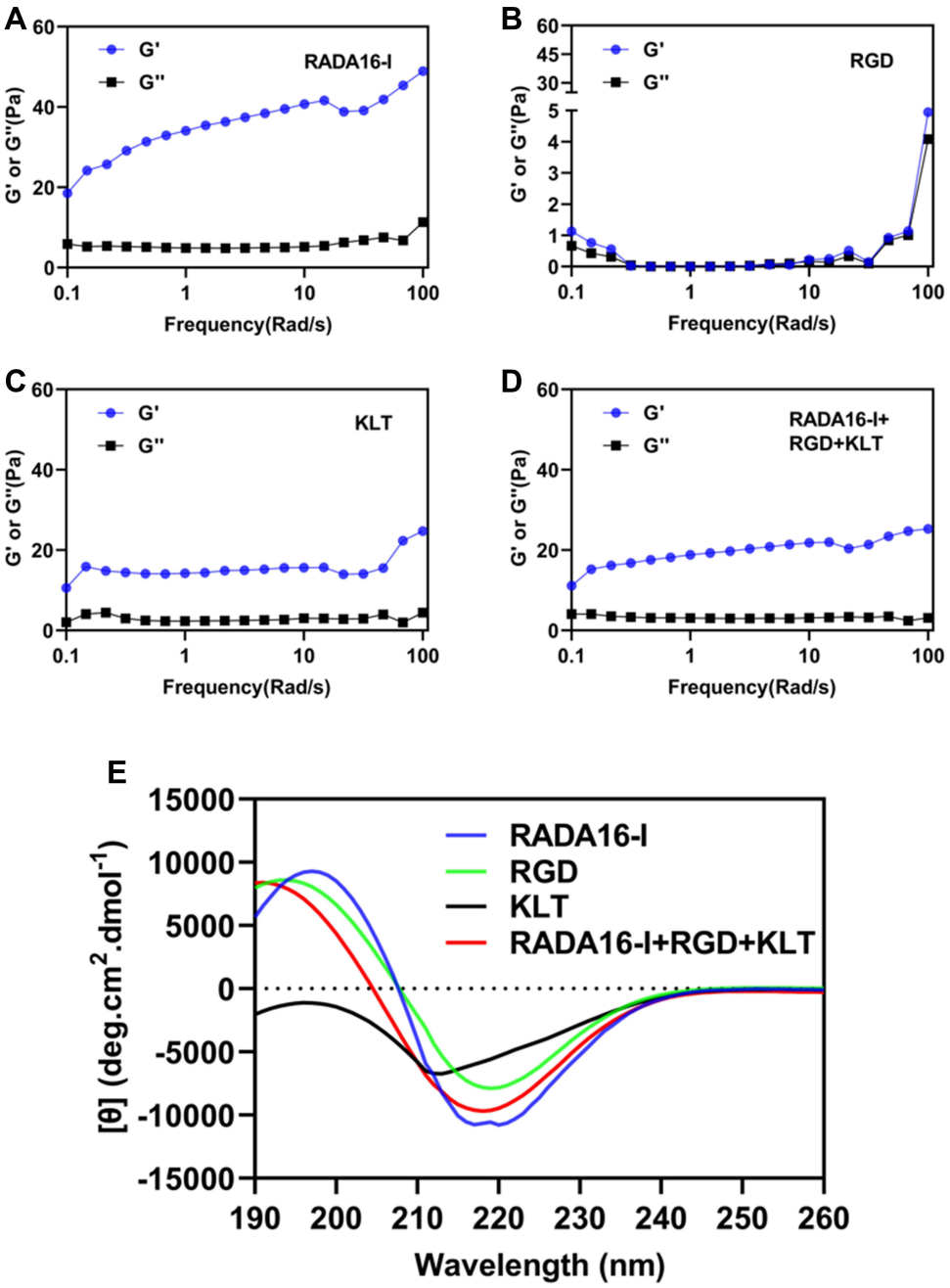

Figure 3 Mechanical properties of peptide hydrogels. Rheological analysis of peptide hydrogels. Storage modulus (G') and loss modulus (G") of four peptide solutions. (**A**) RADA16-I, (**B**) RGD, (**C**) KLT, and (**D**) RADA16-I+RGD+KLT. (**E**) Circular dichroism analysis of the structure of four peptide solutions.

concentration of VEGF in the total intracellular protein was significantly higher than that in the culture supernatant (Figure 2F). This result indirectly confirmed that hydrogels significantly increased intracellular VEGF secretion.

Treatment of Skin Wounds Using Hydrogel-Loaded hUC-MSCsp

Cell-free peptide hydrogels have been used as a matrix to accelerate diabetic wound healing.[18] To examine the synergistic effect of hydrogels and hUC-MSCsp, the wounds were filled with PBS, hUC-MSCs, hUC-MSCsp, or hydrogels loaded with hUC-MSCsp. Because all wounds were completely healed within 21 days (Figure 4A), mice were fed for 21 days to assess the quality of wound healing. Wound healing was accelerated after the transplantation of hUC-MSCs, and time to complete healing was reduced from 21 to 18 days compared with the PBS group. In addition, the

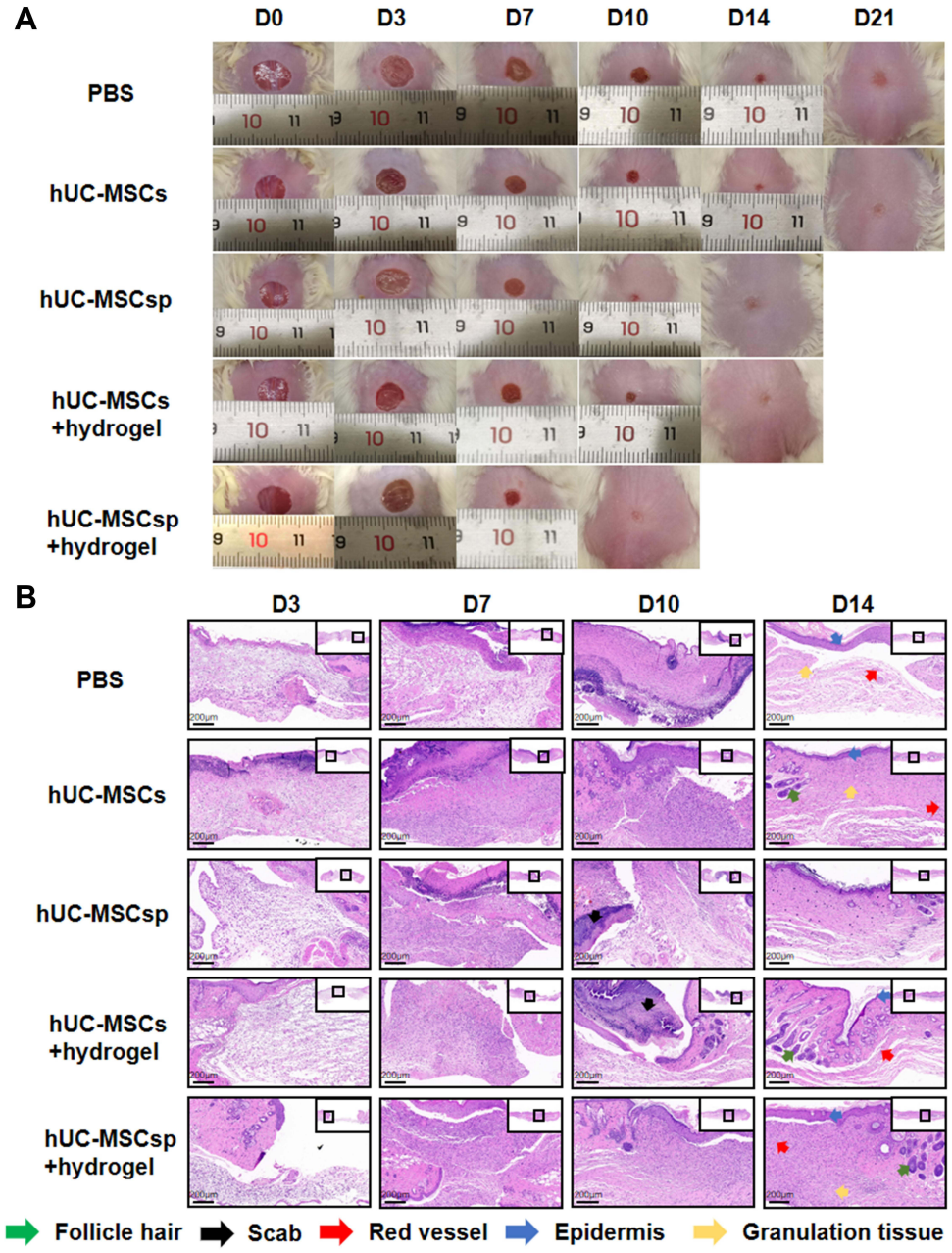

Figure 4 Wound healing behaviors with different treatments. (**A**) Representative photo micrographs of wounds when treated with different treatments administered for various durations. The inner diameter of initial wound was 8 mm. (**B**) Hematoxylin and eosin (H&E) stained images of wounds with different treatments after 3, 7, 10, and 14 days. Green arrow: follicle hair, black arrow: scab, red arrow: red vessel, blue arrow: epidermis, and orange arrow: granulation tissue. Scale bar: 200 μm.

time to complete healing in the hydrogel group loaded with hUC-MSCs and the hydrogel group loaded with hUC-MSCsp was reduced to 14 and 10 days, respectively (Figure 4A). Similar to previous studies, the combined application of peptide hydrogels and hUC-MSCs accelerated tissue[19,20] and organ repair and this synergistic effect between hydrogels and hUC-MSCs provided a better microenvironment. The presence of the hydrogel also maintained cell survival. Cellular activity and paracrine functions in turn allowed the hydrogel to become closer to the microenvironment in which the cells resided, leading to a faster tissue regeneration. The hydrogels loaded with hUC-MSCs and hUC-MSCsp established a synergistic cell-biomaterial ecological niche for the wound and achieved 90% wound closure by day 10 (Figure 6A). The diameters of wounds between groups after 3, 7, and 10 days are shown in Figure 6C. However, HE showed more granulation tissue and faster optimal re-epithelialization in the hUC-MSCsp with hydrogel group compared with the other

groups. The vascular density was also greater compared with the other groups, completely covering the wound on day 10 (Figure 4B). The results confirmed that hUC-MSCsp+hydrogel was the optimal wound healing treatment in this study.

Because we previously labeled the cells using GFP, we used immunohistochemical analysis to track the destination of hUC-MSCs after the mice skin specimens were removed. As shown in Figure 5A, we found more positive labeling, for a longer duration, in the hydrogel containing hUC-MSCsp. Therefore, the compatibility of hydrogels with hUC-MSCs and the greater synergistic effect of co-culture than single hUC-MSCs were also verified. However, although the results were positive, the number was small. It is possible that hUC-MSCs have multidirectional differentiation capacity as well as the ability to promote wound healing through another mechanism, such as paracrine factors. In addition to tracking the cells, we used CD31 to label blood vessels in the fresh skin. Angiogenesis in the trabecular bed was detected by

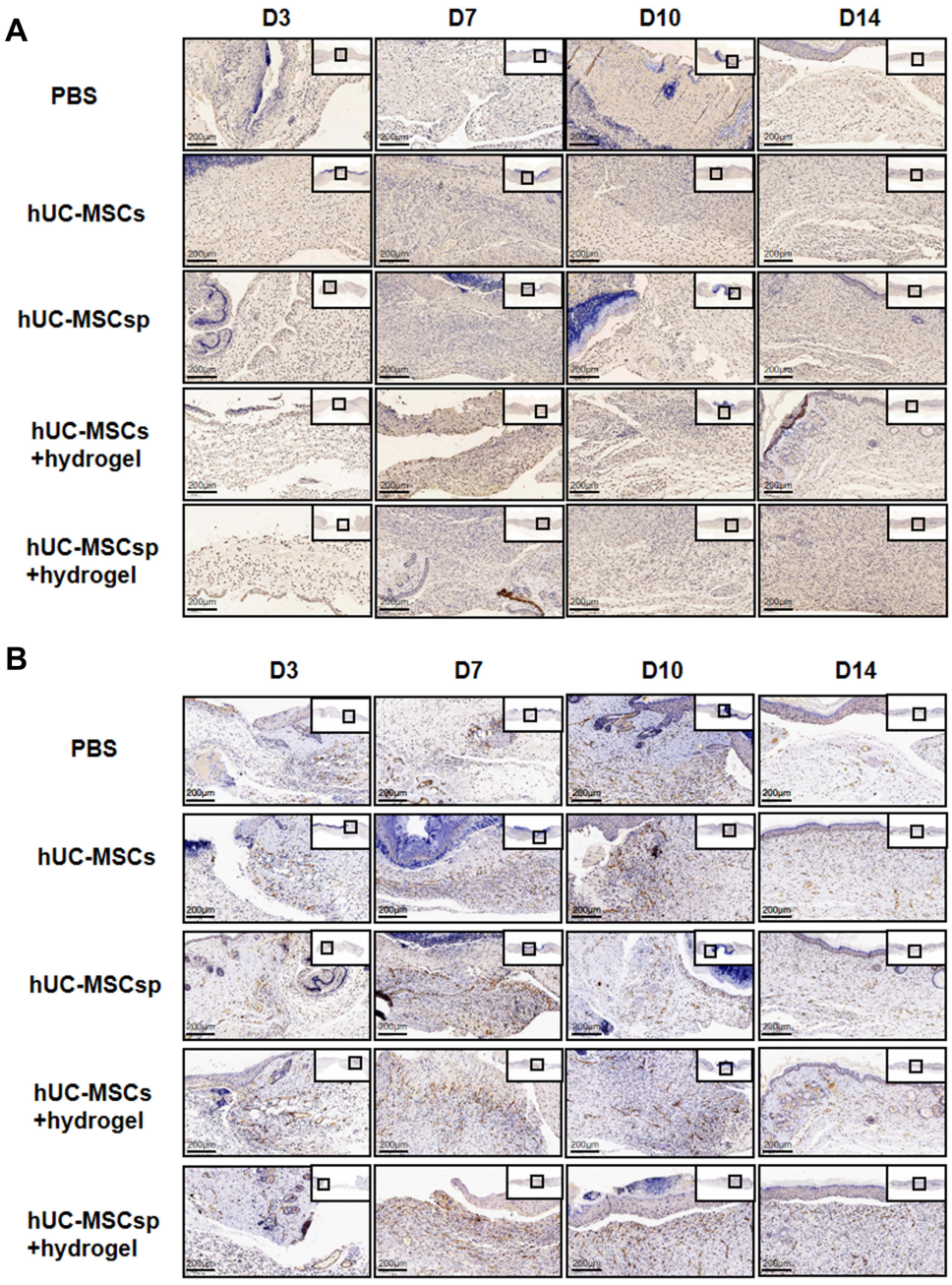

Figure 5 Immunohistochemical analysis of GFP and angiogenesis. (**A**) Representative images of GFP immunohistochemical staining of each group at 3, 7, 10, and 14 days after surgery. Scale bar: 200μm. (**B**) Representative images of CD31 immunohistochemical staining of each group at 3, 7, 10, and 14 days after surgery. Scale bar: 200μm.

immunohistochemical staining for CD31 staining on days 3, 7, 10, and 14 postoperatively. As shown in Figure 5B, on postoperative day 3, microvessels were observed with a typical round or oval shape. Quantitative analysis of microvessels showed that more neovascular microvessels were present in the hUC-MSCsp+hydrogel and hUC-MSCs+hydrogel groups. During the process of wound healing, the density of neovascularization in the fresh skin tissue at the wound was also significantly increased (4.60 ± 0.50 vs 3.85 ± 0.73 vs 3.97 ± 0.64 vs 3.53 ± 0.55 vs 3.22 ± 0.43, $p<0.01$). The difference was most significant between hUC-MSCsp+hydrogel groups and other groups on postoperative day 14 ($p<0.05$) (Figure 6B and D). Taken together, these results demonstrate that a combination of cellular spheroids and hydrogel promoted angiogenesis, which in turn accelerated wound healing.

Previous studies have shown that the promotion of wound healing occurred indirectly through paracrine secretion from MSCs. IL-6, IL-1β, and TNF-α are pro-inflammatory factors, and IL-10 is an anti-inflammatory factor, all of which have an important role in the inflammatory response.[21,22] Therefore, we assessed the secretion patterns of these important cytokines (IL-6, IL-10, IL-1β, and TNF-α) during wound healing by ELISA and found that IL-6, IL-10, IL-1β, and TNF-α were increased and then decreased (Figure 6E–H). The secretions of IL-6, IL-1β, and TNF-α were significantly inhibited in the hUC-MSCs+hydrogel groups compared with the other groups. The concentration of IL-10 in the PBS group was consistently higher during the wound healing process. However, for the hUC-MSCs, hUC-MSCsp, and hUC-MSCs+hydrogel groups, the concentration of IL-10 decreased during the later stages of wound healing. For the hUC-MSCsp+hydrogel group, IL-10 was at a lower level compared with the other groups. Thus, hUC-MSCsp co-cultured with hydrogel significantly inhibited the secretion of IL-10. These analyses of IL-6, IL-10, IL-1β, and TNF-α showed that the combination of hUC-MSCsp and hydrogel significantly reduced the secretion of inflammatory factors during the treatment of skin wounds.

Discussion

Stimulation of the extracellular environment promoted the proliferation and differentiation potential of mesenchymal stem cells (MSCs).[23] Therefore, MSCs are now often transplanted directly into target tissues or stimulated to differentiate into mature tissues for the purpose of repairing defective tissues.[24] However, there are limitations to this approach, including low differentiation efficiency, the uncontrollable direction of differentiation, and the potential for tumor-like transformation. The strong paracrine capability of MSCs provides a new approach to tissue repair.[25] Previous studies reported that a combination of stem cells and vector biomaterials jointly constituted a growth pattern conformed to the internal environment of the human body; thus, greatly improving the survival rate and proliferation efficiency of MSCs, and significantly enhancing their secretory properties.[26,27] There have been a number of studies on the tissue engineering of vector biomaterials, mainly involving bio-ceramics, alginate, chitosan, and hydrogels. Cell sheets, nanoparticles, and 3D printing technologies were also shown to be important. Previous studies showed that hydrogels combined with stem cells provided better repair effects in muscle injury, nerve injury, and myocardial infarction.[28,29] In this study, we used injectable self-assembled nanopeptide hydrogels assembled into various shapes to adapt to skin damage, which could also be injected into tissues for repair.

Studies have previously mixed MSC suspensions directly with biocarrier materials. Recent studies suggest that facilitating the in vitro assembly of MSCs into spheroids may be an effective strategy, but there have been few studies on the binding of MSC spheroids to carrier materials.[30] In this study, hUC-MSCs were spheroidized, combined with hydrogel in vitro, and the stereospecific structure of hydrogel-hUC-MSCsp was found to be similar to the structure of skin. After the transplantation of hydrogel-hUC-MSCsp into the skin wound mice model, the healing rate was much higher than that of the control group. ELISA also showed that the secretory function of hUC-MSCsp was significantly enhanced compared with the directly transplanted hUC-MSCs group. This suggested that stem cell spheroids had enhanced differentiation potential and secretion capability. Hydrogel as a carrier can provide a three-dimensional environment for the proliferation and secretion of stem cell spheroids. The interaction with MSCs could in turn promote their differentiation potential and secretion capability. Therefore, the combination of stem cell spheroids and vector biomaterials can greatly improve the repair efficiency of stem cells. This might be a potential effective therapeutic strategy for wound repair.

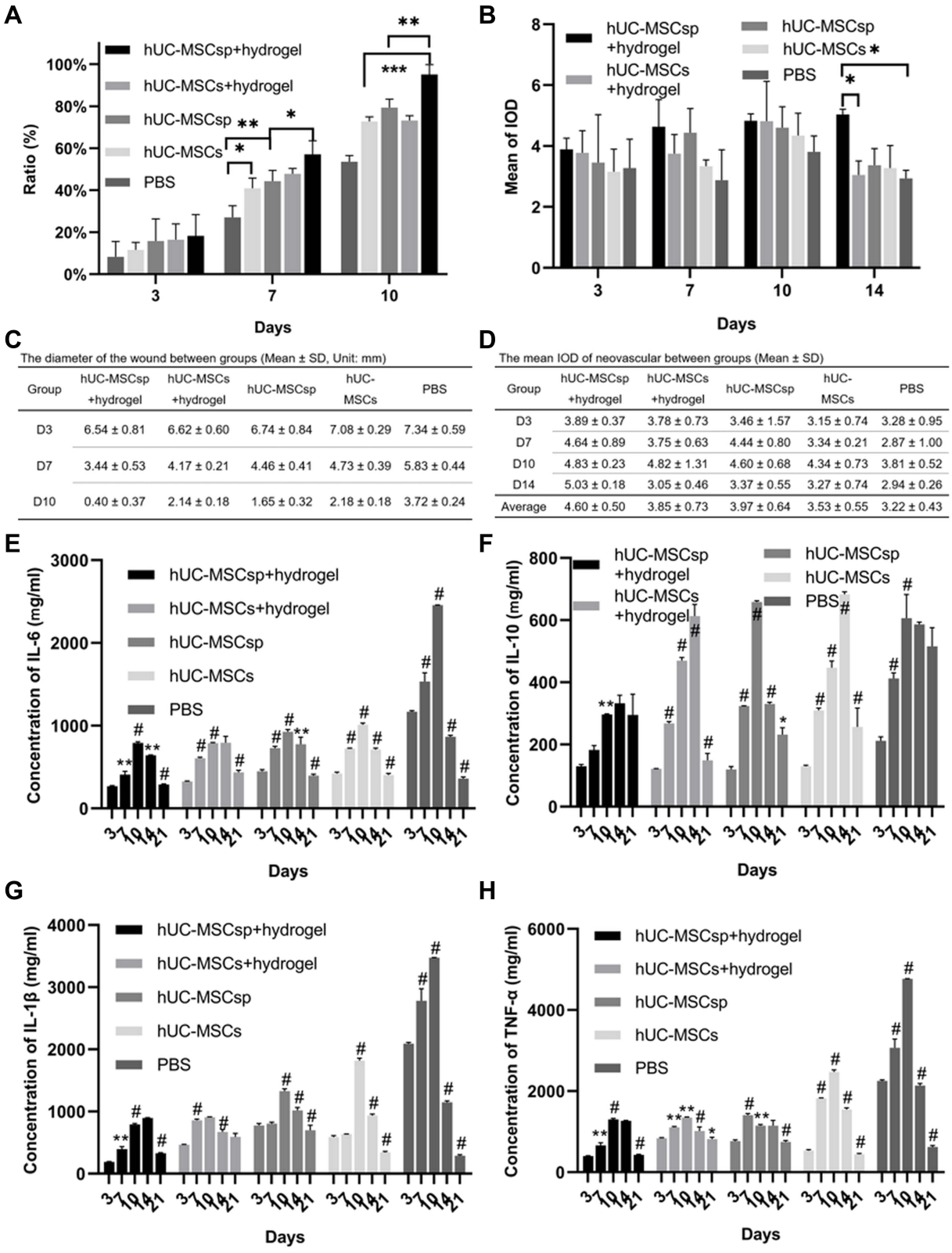

Group	hUC-MSCsp +hydrogel	hUC-MSCs +hydrogel	hUC-MSCsp	hUC-MSCs	PBS
D3	6.54 ± 0.81	6.62 ± 0.60	6.74 ± 0.84	7.08 ± 0.29	7.34 ± 0.59
D7	3.44 ± 0.53	4.17 ± 0.21	4.46 ± 0.41	4.73 ± 0.39	5.83 ± 0.44
D10	0.40 ± 0.37	2.14 ± 0.18	1.65 ± 0.32	2.18 ± 0.18	3.72 ± 0.24

Group	hUC-MSCsp +hydrogel	hUC-MSCs +hydrogel	hUC-MSCsp	hUC-MSCs	PBS
D3	3.89 ± 0.37	3.78 ± 0.73	3.46 ± 1.57	3.15 ± 0.74	3.28 ± 0.95
D7	4.64 ± 0.89	3.75 ± 0.63	4.44 ± 0.80	3.34 ± 0.21	2.87 ± 1.00
D10	4.83 ± 0.23	4.82 ± 1.31	4.60 ± 0.68	4.34 ± 0.73	3.81 ± 0.52
D14	5.03 ± 0.18	3.05 ± 0.46	3.37 ± 0.55	3.27 ± 0.74	2.94 ± 0.26
Average	4.60 ± 0.50	3.85 ± 0.73	3.97 ± 0.64	3.53 ± 0.55	3.22 ± 0.43

Figure 6 Quantitative analysis of different indexes of each group. (**A**) Quantification of wound healing rates of each group. (**B**) Quantitative analysis of the mean of IOD of each region in each group after 3, 7, 10, and 14 days. (**C**) Comparison of the diameters of wounds between groups. (**D**) The mean IOD of neovascularization between groups. Quantification of (**E**) IL-6, (**F**) IL-10, (**G**) IL-1β, and (**H**) TNF-α concentrations in each group. Data are presented as the mean ± SD and error bars indicate the SD. P-values were calculated using two-way ANOVA with Tukey's multiple comparison tests. *p<0.05, **p<0.01, ***p<0.001 or #when p<0.001, #indicated it was statistically significant compared with prior data within groups.

Recent studies have shown that hydrogels accelerated diabetic wound healing by promoting epithelialization and angiogenesis through sustained oxygenation and reducing the inflammatory response.[18] The current study showed that hydrogel combined with hUC-MSCsp greatly inhibited the paracrine capability of stem cells. The expression levels of pro-inflammatory factors were significantly decreased, with over 50% reduction in secretion levels, and the expression levels of anti-inflammatory factors were also reduced. A significant increase in the density of neovascularization was also found. The expression of markers associated with neovascularization, including VEGF and CD31, were significantly enhanced. This suggested that the hydrogel loaded with hUC-MSCs promoted neovascularization and facilitated the repair of skin injury. The proliferation curves of hUC-MSCs showed that the survival and proliferation rates of MSCs were also significantly increased after combination with hydrogel, indicating that the hydrogel provided an extremely favorable environment for the survival and growth of MSCs. Overall, the combination of hUC-MSCsp with the vector biomaterial regulated the inflammatory response and effectively stimulated vascular neogenesis, thus accelerating the injury repair.

There were several limitations in this study. The mechanisms of the interaction between hUC-MSCsp and hydrogel and how hUC-MSCsp exerts a stronger differentiation and secretion potential than hUC-MSCs alone need further investigation. The mechanism by which hUC-MSCs spheroids promote angiogenesis and modulate the inflammatory response also need clarification. The inflammatory response includes a variety of inflammatory factors, and further studies should detect and validate a broader range of relevant inflammatory factors.

Conclusion

This study demonstrated that self-assembled nanopeptide hydrogels loaded with hUC-MSCsp greatly accelerated diabetic skin wound healing with high efficiency of repair. The combination of hUC-MSCsp with the hydrogel exhibited superior efficacy of faster healing by downregulating inflammatory factors to modulate the inflammatory response and upregulating VEGF to promote angiogenesis. Thus, this approach is expected to provide an effective strategy to accelerate chronic diabetic wound healing without the use of drugs in a clinical setting and help the design of novel wound healing agents. In the future, we will improve the efficiency of stem cell spherification and elucidate the underlying mechanisms further.

Abbreviations

AFM, atomic force microscopy; CD, circular dichroism; CLSM, confocal laser scanning microscopy; CCK-8, cell counting kit-8; DM, diabetes mellitus; DAB, diaminobenzidine; DMEM, Dulbecco's Modified Eagle's Medium; EDTA, ethylene diamine tetraacetic acid; ELISA, enzyme-linked immunosorbent assay; FBS, fetal bovine serum; GFP, green fluorescent protein; hUC-MSCs, Human umbilical cord mesenchymal stem cells; hUC-MSCsp, human umbilical cord mesenchymal stem cell spheroids; HE, hematoxylin and eosin; IL, interleukin; IOD, integral optical density; G", loss modulus; MSCs, mesenchymal stem cells; MOI, multiplicity of infection; PMSF, phenylmethanesulfonyl fluoride; PBS, phosphate buffer saline; RIPA, radioimmunoprecipitation assay buffer; G', storage modulus; SD, standard deviation; SEM, scanning electron microscopy; TNF, tumor necrosis factor; VEGF, vascular endothelial growth factor.

Data Sharing Statement

The datasets used and/or analyzed during the current study are available from the corresponding author on reasonable request.

Ethics Approval

The animal experiments were approved by the Ethics Committee of Shandong University Qilu Hospital and were conducted in accordance with the ethical guidelines and in compliance with the National Institutes of Health Guide for the Care and Use of Laboratory Animals. (ethics number: KYLL-KS-2021101).

Acknowledgments

We thank J. Ludovic Croxford, PhD, from Liwen Bianji (Edanz) (www.liwenbianji.cn/) for editing the language of a draft of this manuscript.

Author Contributions

Junshuai Xue was responsible for the acquisition, experiment, analysis, and interpretation of data and drafted the paper. Nianfeng Sun and Yang Liu were responsible for the design of the study, interpretation of data, and drafted the paper and substantively revised it, as well as being the co-correspondence author.

Funding

This report was supported by National Natural Science Foundation of China (Grant No.82000451) and Shandong Provincial Natural Science Foundation (Grant No. ZR2017MH072).

Disclosure

The authors declare that they have no competing interests.

References

1. American Diabetes Association. Standards of medical care in diabetes–2012. *Diabetes Care*. 2012;35(Suppl1):S11–S63. doi:10.2337/dc12-s011
2. Chamberlain JJ, Rhinehart AS, Shaefer CF Jr, Neuman A. Diagnosis and management of diabetes: synopsis of the 2016 American Diabetes Association standards of medical care in diabetes. *Ann Intern Med*. 2016;164(8):542–552. doi:10.7326/M15-3016
3. Pafili K, Papanas N, Maltezos E. Treatment of diabetic complications: how can we learn by seeking and blundering? *Angiology*. 2015;66 (4):301–303. doi:10.1177/0003319714544948
4. American Diabetes Association. 11. Microvascular complications and foot care: standards of medical care in diabetes-2019. *Diabetes Care*. 2019;42(Suppl 1):S124–S138. doi:10.2337/dc19-S011
5. Maleki H, Khoshnevisan K, Sajjadi-Jazi SM, et al. Nanofiber-based systems intended for diabetes. *J Nanobiotechnology*. 2021;19(1):317. doi:10.1186/s12951-021-01065-2
6. Damayanti RH, Rusdiana T, Wathoni N. Mesenchymal stem cell secretome for dermatology application: a review. *Clin Cosmet Investig Dermatol*. 2021;14:1401–1412. doi:10.2147/CCID.S331044
7. English K, French A, Wood KJ. Mesenchymal stromal cells: facilitators of successful transplantation? *Cell Stem Cell*. 2010;7(4):431–442. doi:10.1016/j.stem.2010.09.009
8. Langer R, Vacanti JP. Tissue engineering. *Science*. 1993;260(5110):920–926. doi:10.1126/science.8493529
9. Wang P, Zhao L, Chen W, Liu X, Weir MD, Xu HH. Stem cells and calcium phosphate cement scaffolds for bone regeneration. *J Dent Res*. 2014;93 (7):618–625.
10. Wang W, Lu KJ, Yu CH, Huang QL, Du YZ. Nano-drug delivery systems in wound treatment and skin regeneration. *J Nanobiotechnology*. 2019;17 (1):82. doi:10.1186/s12951-019-0514-y
11. Lima TPL, Passos MF. Skin wounds, the healing process, and hydrogel-based wound dressings: a short review. *J Biomater Sci*. 2021;32 (14):1910–1925. doi:10.1080/09205063.2021.1946461
12. Yang J, Chen Z, Pan D, Li H, Shen J. Umbilical cord-derived mesenchymal stem cell-derived exosomes combined pluronic F127 hydrogel promote chronic diabetic wound healing and complete skin regeneration. *Int J Nanomedicine*. 2020;15:5911–5926. doi:10.2147/IJN.S249129
13. Shi Q, Qian Z, Liu D, et al. gmsc-derived exosomes combined with a chitosan/silk hydrogel sponge accelerates wound healing in a diabetic rat skin defect model. *Front Physiol*. 2017;8:904. doi:10.3389/fphys.2017.00904
14. Gelain F, Luo Z, Zhang S. Self-assembling peptide EAK16 and RADA16 nanofiber scaffold hydrogel. *Chem Rev*. 2020;120(24):13434–13460. doi:10.1021/acs.chemrev.0c00690
15. Rao F, Wang Y, Zhang D, et al. Aligned chitosan nanofiber hydrogel grafted with peptides mimicking bioactive brain-derived neurotrophic factor and vascular endothelial growth factor repair long-distance sciatic nerve defects in rats. *Theranostics*. 2020;10(4):1590–1603. doi:10.7150/thno.36272
16. Yang M, Zhang ZC, Liu Y, et al. Function and mechanism of RGD in bone and cartilage tissue engineering. *Front Bioeng Biotechnol*. 2021;9:773636. doi:10.3389/fbioe.2021.773636
17. Mo M, Wang S, Zhou Y, Li H, Wu Y. Mesenchymal stem cell subpopulations: phenotype, property and therapeutic potential. *Cell Mol Life Sci*. 2016;73(17):3311–3321. doi:10.1007/s00018-016-2229-7
18. Guan Y, Niu H, Liu Z, et al. Sustained oxygenation accelerates diabetic wound healing by promoting epithelialization and angiogenesis and decreasing inflammation. *Sci Adv*. 2021;7(35):35. doi:10.1126/sciadv.abj0153
19. Zhang Z, Li Z, Li Y, et al. Sodium alginate/collagen hydrogel loaded with human umbilical cord mesenchymal stem cells promotes wound healing and skin remodeling. *Cell Tissue Res*. 2021;383(2):809–821. doi:10.1007/s00441-020-03321-7
20. Yao M, Li J, Zhang J, et al. Dual-enzymatically cross-linked gelatin hydrogel enhances neural differentiation of human umbilical cord mesenchymal stem cells and functional recovery in experimental murine spinal cord injury. *J Mater Chem*. 2021;9(2):440–452. doi:10.1039/D0TB02033H
21. Kang S, Kishimoto T. Interplay between interleukin-6 signaling and the vascular endothelium in cytokine storms. *Exp Mol Med*. 2021;53 (7):1116–1123. doi:10.1038/s12276-021-00649-0

22. Ip WKE, Hoshi N, Shouval DS, Snapper S, Medzhitov R. Anti-inflammatory effect of IL-10 mediated by metabolic reprogramming of macrophages. *Science*. 2017;356(6337):513–519. doi:10.1126/science.aal3535
23. Ha DH, Kim HK, Lee J, et al. Mesenchymal stem/stromal cell-derived exosomes for immunomodulatory therapeutics and skin regeneration. *Cells*. 2020;9(5):1157. doi:10.3390/cells9051157
24. Berebichez-Fridman R, Montero-Olvera PR. Sources and clinical applications of mesenchymal stem cells: state-of-the-art review. *Sultan Qaboos Univ Med J*. 2018;18(3):e264–e277. doi:10.18295/squmj.2018.18.03.002
25. Bian D, Wu Y, Song G, Azizi R, Zamani A. The application of mesenchymal stromal cells (MSCs) and their derivative exosome in skin wound healing: a comprehensive review. *Stem Cell Res Ther*. 2022;13(1):24. doi:10.1186/s13287-021-02697-9
26. Wechsler ME, Rao VV, Borelli AN, Anseth KS. Engineering the MSC secretome: a hydrogel focused approach. *Adv Healthcare Mater*. 2021;10(7): e2001948. doi:10.1002/adhm.202001948
27. Lv B, Zhang X, Yuan J, et al. Biomaterial-supported MSC transplantation enhances cell-cell communication for spinal cord injury. *Stem Cell Res Ther*. 2021;12(1):36. doi:10.1186/s13287-020-02090-y
28. Han Y, Li X, Zhang Y, Han Y, Chang F, Ding J. Mesenchymal stem cells for regenerative medicine. *Cells*. 2019;8(8):886. doi:10.3390/cells8080886
29. Raghav PK, Mann Z, Ahlawat S, Mohanty S. Mesenchymal stem cell-based nanoparticles and scaffolds in regenerative medicine. *Eur J Pharmacol*. 2021;918:174657. doi:10.1016/j.ejphar.2021.174657
30. Cesarz Z, Tamama K. Spheroid culture of mesenchymal stem cells. *Stem Cells Int*. 2016;2016:9176357. doi:10.1155/2016/9176357